Geochemical Journal, Vol. 44, pp. 211 to 223, 2010

Mn– and Fe–carbonate rich layers in Meso–Cenozoic shales as proxies of environmental conditions: A case study from the southern Apennine, Italy

GIOVANNI MONGELLI,[1]* SALVATORE CRITELLI,[2] ENRICO DINELLI,[3] MICHELE PATERNOSTER[1] and FRANCESCO PERRI[1]

[1]Dipartimento di Chimica, Università degli Studi della Basilicata, Campus di Macchia Romana, 85100 Potenza, Italy
[2]Dipartimento di Scienze della Terra, Università degli Studi della Calabria, 87036 Arcavacata di Rende (CS), Italy
[3]Dipartimento di Scienze della Terra e Geologico-Ambientali, Università di Bologna, 40126 Bologna, Italy

(*Received April 23, 2009; Accepted September 28, 2009*)

Mn-rich layers and interbedded shales from a well exposed natural section of the Northern-Calabrian Unit (Late Jurassic–Early Oligocene) in the surroundings of the Terranova del Pollino village, southern Italy, have been mineralogically and chemically analyzed, in order to reveal the factors controlling their formation. Mn-rich layers are composed of micas/clay minerals, rhodochrosite, siderite, chlorite and quartz whereas shales are formed by micas, clay minerals, chlorite, quartz, and feldspars. The MnO abundances in the Mn-rich layers, which are depleted relatively to the UCC in SiO_2, TiO_2, Al_2O_3, Na_2O, K_2O, and P_2O_5, are in the range of 11.01 ÷ 18.41 (wt. %). R-mode Factor analysis indicate that SiO_2, Al_2O_3, TiO_2, Na_2O and K_2O have high positive weights in the first factor (59.8% of the total variance) whereas high negative weights are observed for Fe_2O_3, MnO, and CaO. This factor accounts for the competition between the terrigeneous component, the authigenic carbonate phases accumulating Mn and Fe which likely formed during paucity of detrital supply. The negative weight of CaO and MnO in this factor, the higher Ca contents in the Mn-rich layers compared to shales, and the lack of calcite, suggest the presence of a mixed Mn–Ca carbonate rather than pure rhodochrosite. It is generally retained that Ca–rhodochrosite precipitates within the pore waters of reducing sediments since neither rhodochrosite nor siderite can form in equilibrium with bottom seawater. Thus the resulting sediment should be a mixing between the detrital component and the authigenic one. Assuming Al_2O_3 as an index of the detrital component, it is clearly envisaged that in the Al_2O_3/MnO vs. Al_2O_3 diagram the carbonate-rich samples fall on the mixing curve having as end members the average shale and the richest MnO sediment. This supports the idea that carbonate-rich samples formed through precipitation of carbonate minerals in the pore waters of the terrigenous detritus accumulating at the sea bottom. Further the REE distribution of unaltered marine carbonates is expected to be representative of ambient seawater where carbonates precipitated. Carbonates normalized to fine-grained siliciclastic sediments, have typical HREE enrichment, negative Ce-anomaly, and lower total REE. In our case, the carbonate-rich samples normalized to the average composition of the interbedded free-carbonate shale, show HREE enrichment, lower total REE contents, and the lack of negative Ce-anomaly, due to the anoxic environment of formation for Mn– and Fe–carbonate. Finally was observed that the mineralization is enhanced if the site of accumulation is protected from dilution by clastic sediment input. The alternation between Mn– and Fe–carbonate silts and carbonate-free shales along the studied sedimentary succession, were likely controlled by eustatic sea-level oscillations which are well documented in the western Tethys during Middle and Late Triassic.

Keywords: geochemistry, manganese, Northern-Calabrian Unit, rhodochrosite, southern Italy

INTRODUCTION

Siderite ($FeCO_3$) and rhodochrosite ($MnCO_3$) are reduced phases occurring in continental and marine deposits (e.g., Kelts, 1998; McMillan and Schwertmann, 1998). The concentration of Fe^{2+} and Mn^{2+} in anaerobic waters is controlled by several factors including equilibrium solubility of mineral phases, kinetic of precipitation reactions, cation exchange, and adsorption processes (Jensen *et al*., 2002). The solubility of siderite and rhodochrosite limits Fe and Mn concentrations under anoxic conditions (e.g., Morgan, 1967; Middelburg *et al*., 1987; Amirbahman *et al*., 1998; Jensen *et al*., 2002) whereas under oxic and mildly alkaline conditions $FeCO_3$ and $MnCO_3$ solubility is complicated by oxidation of aqueous Fe^{2+} and Mn^{2+} and subsequent precipitation of Fe^{III} and $Mn^{III/IV}$ (hydr)oxide minerals, which are orders of magnitude less soluble than the carbonate material (Dresel, 1989; McMillan and Schwertmann, 1998; La Force *et al*., 2002). The interconversions among mineral phases are episodic and seasonal, varying with temporal changes in local Eh and pH (La Force *et al*., 2002).

Dissolution and precipitation are significant in the (bio)geochemical cycling not only of Fe and Mn but also

*Corresponding author (e-mail: mongelli@unibas.it)

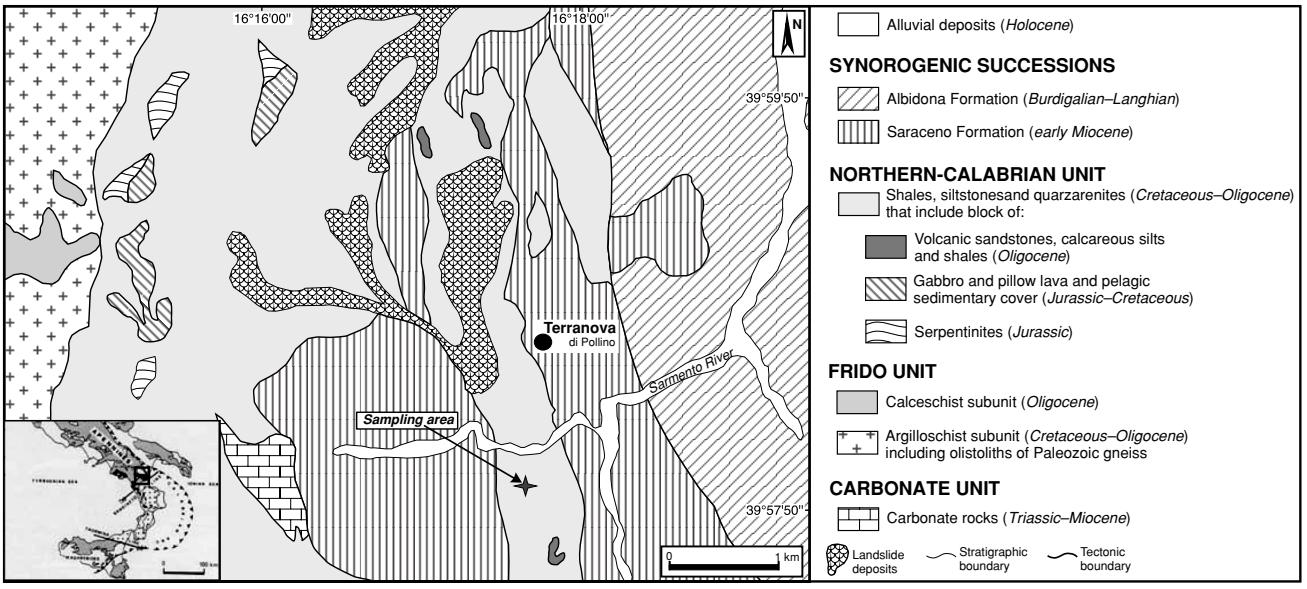

Fig. 1. Geological sketch map of the southern Apennines (Italy), in the surroundings of the Terranova del Pollino village. Location of the sampling area (modified from Monaco et al., 1995).

of other metals (e.g., U, Co, Pb, Ni, Cu, and Zn) that coprecipitate with Fe and Mn (hydr)oxides (Hem, 1978; Hem *et al*., 1989; Duff *et al*., 2002). In the natural environment, cycling of Fe and Mn occurs at oxic/anoxic interfaces where precipitation and dissolution occur simultaneously. In modern marine sediments, Mn is present above its crustal abundance as an oxyhydroxide in all slowly accumulating (pelagic) sediments of the deep ocean and in surficial deposits of continental margin environments. Diagenetic recycling of Mn in the latter causes surficial deposits to have larger Mn enrichments than in many pelagic sediments. Bottom sediments of permanently anoxic basins show no enrichments and have Mn concentrations that are controlled solely by the aluminosilicate fraction. Manganese carbonates are found only in anoxic sediments accumulating beneath surface oxic horizons (and therefore under oxygenated bottom waters) in many nearshore environments. Such enrichments are due to delivery of Mn by burial of surface oxyhydroxides into the subsurface anoxic environment where they are dissolved. The presence of Mn carbonates therefore signifies that the host sediment must have accumulated under oxygenated bottom waters. On the basis of this information it is proposed that, in contrast to several current explanations for the formation of Mn carbonates in ancient organic-rich shales, limestone, and marl sequences and in many Mn ore deposits, the occurrence of these mineral phases indicates that the sediments originally accumulated beneath oxygenated bottom waters (Calvert and Pedersen, 1996).

The peak of dissolved Mn concentrations occurring around the anoxic/oxic boundary and Mn–carbonate may "encircle" areas of black shale deposition if the interface remains stable over geological time (Bolton and Frakes, 1985; Force and Cannon, 1988). However, since Mn concentrations in modern anoxic basins are lower than necessary for its precipitation as carbonate (Calvert and Pedersen, 1996), alternative models were proposed including diagenetic formation (Jenkyns, 1988; Pedersen and Calvert, 1990; Calvert and Pedersen, 1996), contribution of both direct precipitation from sea-water and organic matter mediated diagenetic formation (e.g., Öztürk and Hein, 1997; Zeng and Liu, 1999; Fan *et al*., 1999; Yeh *et al*., 1999), and diagenetic reaction of limestone with Mn–oxyhydroxides (Dasgupta *et al*., 1992).

Sedimentary deposits enriched in Mn mineralization are found in many Apennine ophiolite complexes (Bonatti *et al*., 1976; Boni and di Nocera, 1977; Marchesini and Pagano, 2001). This paper discusses, for the first time, the peculiar occurrence of Mn–carbonate ores, coupled to Fe–carbonate, in deep-marine shales from the Northern-Calabrian Unit (southern Apennine), a tectonic mélange of the Paleogene oceanic accretionary prism in the southern Italy orogenic system.

GEOLOGICAL SETTING

The mountain physiography of southern Italy consists of tectonically juxtaposed thrust belts belonging to different paleotectonic domains corresponding to the African continental margin (to the east), an oceanic branch of the Neotethyan Ocean, and the European continental

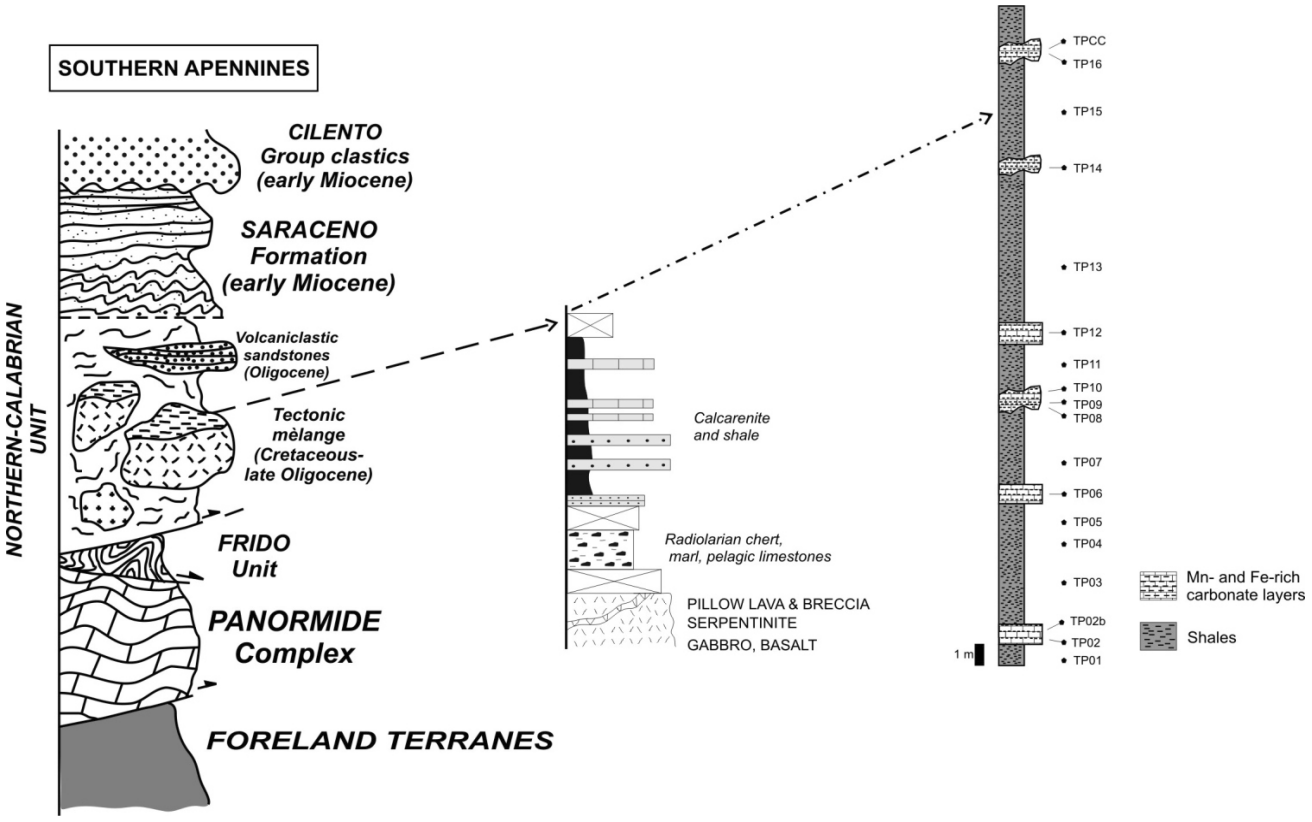

Fig. 2. Stratigraphic column of the studied area. TP01 to TPCC mudstone samples used for mineralogical and geochemical analyses.

margin (to the west) (e.g., Critelli, 1993, 1999). In particular, the southern Apennines are an east-verging accretionary wedge developed in Neogene times above a west-dipping subduction of the Apulian Ionian lithosphere (Doglioni *et al*., 1996). The southern Apennines and northern Calabria are associated with the Tyrrhenian backarc basin, and are characterized by a frontal active accretionary wedge, below sea-level, whereas the main elevated ridge to the west is in uplift and extension. The tectonic style is dominated by a large-scale duplex system, consisting of a complex architecture of carbonate units derived from the internal Apulia platform overlain by rootless nappes (e.g., Patacca and Scandone, 2007 and reference therein).

The subduction of the Adria oceanic lithosphere, activated for all the Paleogene and lower Miocene, producing a diffuse calcalkaline volcanism in Sardinia. Intracontinental rifting occurred in Sardinia during the Oligocene to Miocene. Subduction-related volcanism (between 32 and 11 Ma) was widespread along the western side of Sardinia (Assorgia *et al*., 1988). This volcanism was subdivided in two main phases: calcalkaline eruptions of lavas, from 32 to 26 Ma, and explosive eruptions, which alternated or were contemporaneous with effusive events, between 23 and 11 Ma (Beccaluva *et al*., 1985). The volcanic products of the first phase are andesite, basaltic andesite and basalt, whereas the second phase includes pyroclastic rocks of felsic composition (dacite to rhyolite).

Paleogeographic restorations have been proposed by many authors with different models and interpretations (Ogniben, 1969; Scandone, 1972; Sgrosso, 1986; Pescatore *et al*., 1999; Monaco *et al*., 1995; Patacca and Scandone, 2007). The units derived from deformation of different paleogeographic domains (from platform to basin), represent three tectonostratigraphic key within the Southern Italy orogenic system: 1, the Calabrian Arc (Calabride Units), representing deformation, exhumation and accretion of the European continental margin; 2, the Liguride tectonostratigraphic units (Ogniben, 1969), representing the rests of the Neotethyan Ocean; and 3, the Adria domain, representing different tectonostratigraphic units of the African continental margin (e.g., Critelli and Le Pera, 1998). A recent palinspastic restoration (Cello *et al*., 1996) suggests the existence in the western Mediterranean area, during Late Jurassic time, of an Iberian promontory bordered by the Tethyan Ocean to the south and by a narrow basin, floored by oceanic crust, to the

north. The wider oceanic area south of the promontory is retained as the source region for the material which accreted in the Liguride tectonic wedge up to the early Miocene (Ogniben, 1969), when it collided with the most internal domains of the future southern Apennines (Critelli and Le Pera, 1998). Presently this tectonic wedge forms the allochtonous terranes that, in the southern Apennines, consists of the Frido Unit (Late Jurassic–late Oligocene) and the Northern Calabrian Unit (Late Jurassic–late Oligocene), followed unconformably upward by early Miocene turbiditic synorogenic sequences (Fig. 1). The depositional facies and basin geometry of these tectonostratigraphic units are intensely deformated. In northern Calabria, these units tectonically overly the Apenninic carbonate unit of the Panormide Complex. It is in thrust contact with the overlaying crystalline units of the Calabride Complex. The Northern-Calabrian Unit (Fig. 2) consists of a tectonic mélange that includes fragments of ophiolites (pillow lava, gabbro, serpentinite), andesite and dacite blocks, subarkose and volcanolithic sandstone strata, an oceanic cover of argillaceous chert, radiolarian chert, marl, pelagic limestone, calcarenite, shale and calcareous rocks, and siliciclastic strata (shale, siltstone and sandstone) (e.g., Critelli, 1993). The Frido Unit is composed of calc-schist, slate and phyllite, quartzite, marls, meta-pillow lava, serpentine and shales, and include blocks of garnet-rich gneiss and granite (e.g., Critelli, 1993; Monaco *et al.*, 1995). Moreover, synorogenetic successions (Fig. 1) outcrop along the studied area, and consist of turbiditic calcilutites and calcarenites with interbedded marls, sandstones and microconglomerates.

Methods and Sampling

Ten Mn-rich samples (TP02, TP02b, TP06, TP08, TP09, TP10, TP12, TP14, TP16, TPCC) and eight shales (TP01, TP03, TP04, TP05, TP07, TP11, TP13, TP15) were collected from a well-exposed natural section of the Northern-Calabrian Unit (Fig. 2), in the surroundings of the Terranova del Pollino village. The stratigraphic position of the samples is presented in Fig. 2.

The whole-rock samples were first dried and then crushed by hand in an agate mortar. Randomly-oriented whole-rock powders were run in the 3–66°2θ interval, at a scan speed of 1°2θ/min, with a step size of 0.01°2θ and a counting time of 0.14 sec per step, using a Bruker D8 advance diffractometer equipped with a Cu tube anode. The tube current and the voltage were 40 mA and 40 kV, respectively. The intensities and diffraction angles of the identified minerals were compared to the database of the International Center for Diffraction Data (ICDD).

Major elements, Cu, Nb, Ni, Pb, V, and Zr contents have been analyzed by XRF on powder pellets, following the matrix correction methods of Franzini *et al.*, (1972, 1975) and Leoni and Saitta (1976). Average errors of trace elements are less than ±5% except for those elements at 10 ppm and lower (±5–10%). The estimated precision and accuracy for trace elements determinations are better than 5%, except for those elements having a concentration of less than 10 ppm (10–15%). Total loss on ignition (LOI) was gravimetrically estimated after overnight heating at 950°C.

Ba, Co, Cr, Cs, Rb, Sc, Sr, Th, U, Zn, La, Ce, Nd, Sm, Eu, Tb, Yb, Lu, and Y contents were obtained by Instrumental neutron activation analysis (INAA) at the Activation Laboratories, Ancaster, Canada. Average errors for these elements range from ±5% to ±20% for different elements.

Geochemistry

The elemental concentrations are given in Table 1. The elemental distributions, normalized to the Upper Continental Crust (UCC, Taylor and McLennan, 1985; Rudnick and Fountain, 1995) are shown in Fig. 3.

The interelemental relationships have been evaluated using R-mode factor analysis. The factors have been extracted by Principal Component Analysis (PCA) using the StatView® package. This operation has been performed on the correlation matrix, thus weighing all the variables equally, and allowing us to convert the principal component vectors into factors. The factor loadings arranged as in Table 2 form the factor matrix. The communalities provide an index of the efficiency of the proposed set of factors (Davis, 1986) and the magnitude of the communalities here calculated suggests that most of the original variance is still accounted by our set of factors. Two factors (Table 2) explain 71.1% of the total variance associated with the chemical database (major and trace elements) of the analyzed samples.

Major elements

The Fe- and Mn-rich samples are depleted, relatively to the UCC. SiO_2, TiO_2, Al_2O_3, Na_2O, K_2O, and P_2O_5. MnO, whose abundances are in the range 11.0 to 18.41 wt. %, is notably enriched (150 ÷ 300 × UCC). Fe is enriched (3 ÷ 8 × UCC) whereas MgO is generally close to the UCC value or moderately enriched. CaO is either depleted or close to the UCC value (Fig. 3a).

The shales are characterized by narrow compositional changes for the major elements. SiO_2, TiO_2, Al_2O_3, Fe_2O_3, MnO and MgO have concentrations comparable to those of the UCC whereas alkalis and P_2O_5 are depleted (Fig. 3a). These features are very similar to those observed for other shales in the area (Mongelli and Dinelli, 2001). The samples TP04 and TP11 have higher MnO abundances (0.36 and 0.27 wt. %, respectively), whereas the average

Table 1. Major and trace element in studied samples. Samples TP01, TP03, TP04, TP05, TP07, TP11, TP13, TP15 are shales. TP02, TP02b, TP06, TP08, TP09, TP10, TP12, TP14, TP16, TPCC are Mn-rich layers. Eu/Eu = $Eu_{ch}/\sqrt{Sm_{ch}\cdot Gd_{ch}}$, Gd_{ch} calculated as $2/3Tb_{ch} + 1/3Sm_{ch}$ (Taylor and McLennan, 1985). Chondrite values are from Taylor and McLennan (1985).*

Samples	TP01	TP02	TP02b	TP03	TP04	TP05	TP06	TP07	TP08	TP09	TP10	TP11	TP12	TP13	TP14	TP15	TP16	TPCC
Oxides (wt. %)																		
SiO_2	73.73	23.89	20.20	74.14	68.52	74.22	26.51	76.61	28.65	33.94	21.41	70.72	39.61	71.56	46.61	69.73	32.80	27.79
TiO_2	0.45	0.15	0.12	0.50	0.60	0.52	0.23	0.43	0.17	0.26	0.16	0.56	0.31	0.59	0.17	0.52	0.17	0.14
Al_2O_3	10.15	5.18	5.05	10.84	12.07	10.78	6.57	9.22	7.75	9.04	6.59	11.64	8.50	12.08	4.66	11.01	5.65	3.90
Fe_2O_3	6.01	23.98	23.87	4.44	5.15	4.75	19.35	4.95	18.55	18.25	20.37	5.52	16.56	5.12	15.74	7.90	15.10	34.35
MnO	0.10	16.86	18.41	0.10	0.36	0.09	15.78	0.09	13.10	12.93	20.53	0.27	11.01	0.11	14.32	0.11	17.29	16.06
MgO	3.18	4.08	4.83	2.56	3.00	2.79	5.12	2.77	6.51	5.72	5.36	3.24	4.23	2.67	2.53	4.20	4.08	1.51
CaO	0.33	2.73	2.72	0.43	1.28	0.32	5.64	0.24	4.05	1.85	3.59	0.69	1.96	0.25	1.69	0.31	4.94	0.86
Na_2O	0.17	0.00	0.00	0.27	0.33	0.19	0.00	0.16	0.00	0.00	0.00	0.24	0.10	0.32	0.03	0.13	0.00	0.00
K_2O	1.44	0.27	0.12	1.85	2.09	1.77	0.45	1.36	0.35	0.68	0.35	1.87	0.86	2.14	0.47	1.47	0.48	0.38
P_2O_5	0.08	0.08	0.08	0.09	0.10	0.09	0.14	0.08	0.05	0.07	0.11	0.09	0.07	0.07	0.10	0.06	0.11	0.07
LOI	4.35	22.77	24.58	4.77	6.47	4.48	20.20	4.08	20.80	17.25	21.53	5.15	16.76	5.09	13.66	4.53	19.36	14.93
Total	99.99	99.99	99.99	99.98	99.97	99.99	99.99	99.99	99.98	99.98	99.99	99.99	99.97	99.99	99.99	99.97	99.99	99.99
Trace elements (ppm)																		
V	91	44	39	108	122	98	64	84	71	81	59	107	104	109	45	95	58	39
Cr	72	33	22	81	93	75	39	67	24	39	25	42	53	98	30	90	34	31
Ni	93	50	41	122	124	83	54	90	75	82	64	114	258	73	42	76	55	45
Cu	28	58	53	72	85	37	61	41	39	56	60	60	49	57	52	38	41	65
Rb	85	34	25	107	118	93	37	86	36	44	34	103	56	123	34	89	34	34
Sr	34	98	6	47	69	40	75	35	49	17	20	48	28	45	170	36	80	259
Y	20	16	13	26	27	20	22	17	19	18	21	20	11	19	27	16	39	12
Zr	98	28	24	102	135	108	46	91	40	56	34	117	64	126	34	112	32	27
Nb	13	10	4	11	13	11	8	10	7	8	2	13	8	15	7	12	3	3
Ba	168	83	46	206	203	192	59	162	61	68	58	190	87	209	67	175	67	65
Pb	19	5	14	20	15	12	8	7	23	15	22	16	24	11	25	10	9	26
Co	15	15	14	16	22	17	9	19	15	7	20	17	29	21	12	10	12	13
Cs	4.2	1.3	0.6	5.7	6.3	5.4	1.4	4.3	1.4	1.8	1.1	5.7	2.4	5.7	1.6	4.5	1.3	1.7
Sc	10.8	7.7	6.9	9.9	19.4	12.3	9.9	10.5	17.0	12.8	10.3	13.5	10.6	14.8	12.7	12.9	15.7	6.5
Th	6.2	1.7	1.2	6.7	8.2	7.3	2.4	5.7	1.9	3.0	1.9	6.5	3.2	6.6	1.5	5.9	1.6	1.3
U	1.2	0.5	—	1.6	1.6	1.2	0.7	1.2	0.7	0.6	0.8	1.5	0.7	1.5	0.6	1.0	0.8	0.6
Zn	110	75	75	102	179	79	106	51	113	100	96	107	235	121	77	96	102	58
La	20.9	8.1	6.8	24.2	31.3	23.6	13.4	20.3	9.3	13.6	9.6	28.2	15.9	27.9	10.6	22.4	12.0	7.0
Ce	39	18	14	44	63	43	30	38	20	28	20	55	37	54	23	39	28	18
Nd	18	8	5	19	29	20	11	17	6	12	9	25	13	20	8	17	11	6
Sm	3.55	2.27	1.88	4.57	6.28	4.22	4.21	3.41	2.14	2.48	3.36	4.64	2.98	4.08	2.96	3.28	3.27	2.05
Eu	0.8	0.7	0.5	1.2	1.5	1.0	1.2	0.8	0.6	0.7	0.9	1.0	0.7	0.9	0.8	0.7	0.9	0.6
Tb	nd	nd	0.5	0.7	0.9	nd	0.7	0.6	0.6	0.5	0.5	0.4	nd	nd	0.5	0.5	0.7	nd
Yb	1.8	2.4	2.2	1.8	2.4	1.9	2.0	1.5	4.0	2.7	2.2	2.0	1.4	2.0	3.0	1.6	5.5	2.0
Lu	0.26	0.36	0.35	0.28	0.36	0.28	0.31	0.24	0.62	0.43	0.36	0.31	0.22	0.31	0.48	0.25	0.83	0.31
$(La/Yb)_{ch}$	7.85	2.28	2.09	9.09	8.81	8.39	4.53	9.15	1.57	3.40	2.95	9.53	7.67	9.43	2.39	9.46	1.47	2.37
Eu/Eu*	—	—	0.69	0.79	0.72	—	0.78	0.70	0.60	0.71	0.86	0.93	—	—	0.87	0.90	0.83	—

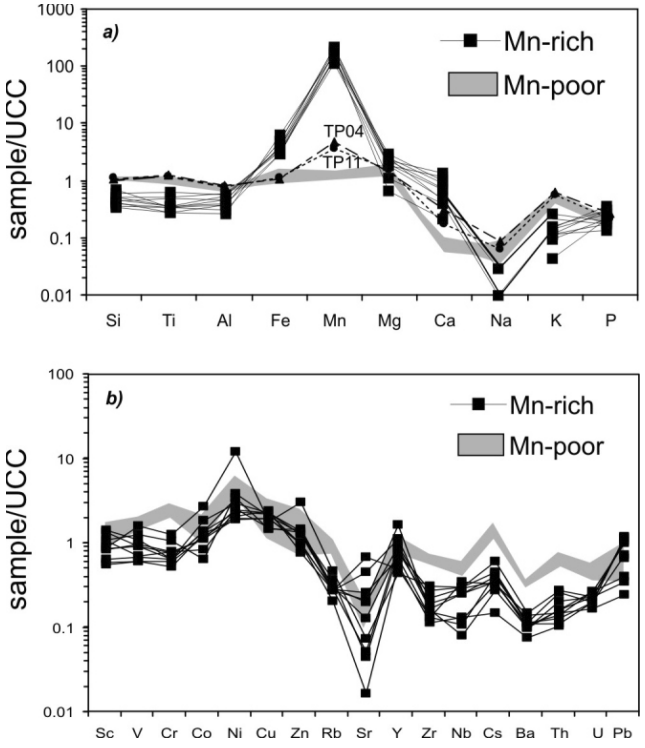

Fig. 3. a) Major and b) trace element compositional ranges normalized to the Upper Continental Crust (UCC, Taylor and McLennan, 1985).

Table 2. R-mode Factor analysis: weights of the variables in the extracted factors. Variables having weight less than 0.60 are omitted.

	F1	F2
SiO_2	0.95	
TiO_2	0.99	
Al_2O_3	0.94	
Fe_2O_3	–0.91	
MnO	–0.97	
CaO	–0.71	
Na_2O	0.96	
K_2O	0.99	
P_2O_5		0.61
V	0.92	
Cr	0.91	
Rb	0.99	
Y		0.87
Zr	0.99	
Nb	0.87	
Ba	0.98	
Cs	0.99	
Th	0.99	
U	0.92	
La	0.98	
Eu	0.60	
Yb		0.68
Var. %	59.8	12.6

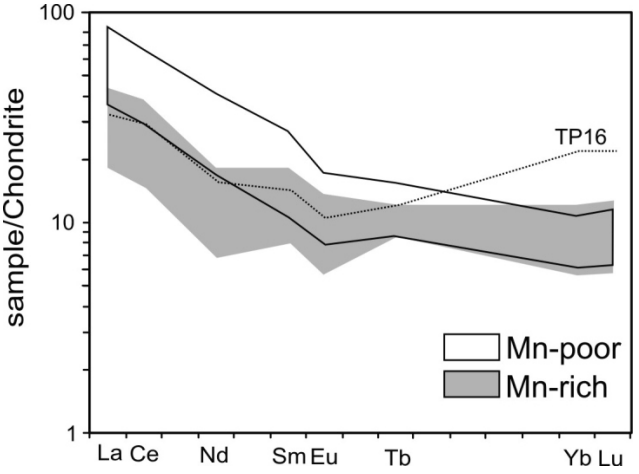

Fig. 4. Rare earth element compositional ranges, chondrite-normalized (Taylor and McLennan, 1985). Sample TP16, showing higher content in HREE, is plotted separately.

MnO content of the remaining shales is 0.10 ± 0.09.

SiO_2, Al_2O_3, TiO_2, Na_2O and K_2O have high positive weights in the first factor obtained by the factor analysis (59.8% of the total variance) whereas high negative weights are observed for Fe_2O_3, MnO, and CaO. This factor accounts for the competition between the terrigeneous component, composed of phyllo- and tectosilicates hosting SiO_2, Al_2O_3, TiO_2, Na_2O and K_2O, and the authigenic carbonate phases accumulating Mn and Fe which likely formed during paucity of detrital supply.

P_2O_5 has not significant weight in the first factor, suggesting that phosphorous is not controlled neither by detrital supply nor by carbonate minerals. It has a positive weight in the second factor (12.6% of the total variance), similarly to some high field strength elements. The second factor could account for secondary precipitation of phosphate phases since P distribution in the sedimentary rocks is often controlled by diagenetic processes (Föllmi, 1996).

Trace elements

Large ion lithophile elements (LILE): Rb, Sr, Cs, Ba, Pb

The Fe- and Mn-rich samples are generally depleted in LILE, relatively to the UCC. In the shales Sr and Ba are depleted whereas Rb, Cs, and Pb have contents close to those of the UCC (Fig. 3b).

Rb, Cs, and Ba have high positive weights in the first factor suggesting they are controlled by detrital minerals. Sr and Pb are instead likely controlled by a sum of factors (e.g., feldspars, calcium carbonates, sheet silicates). This may explain the lack of significant weights

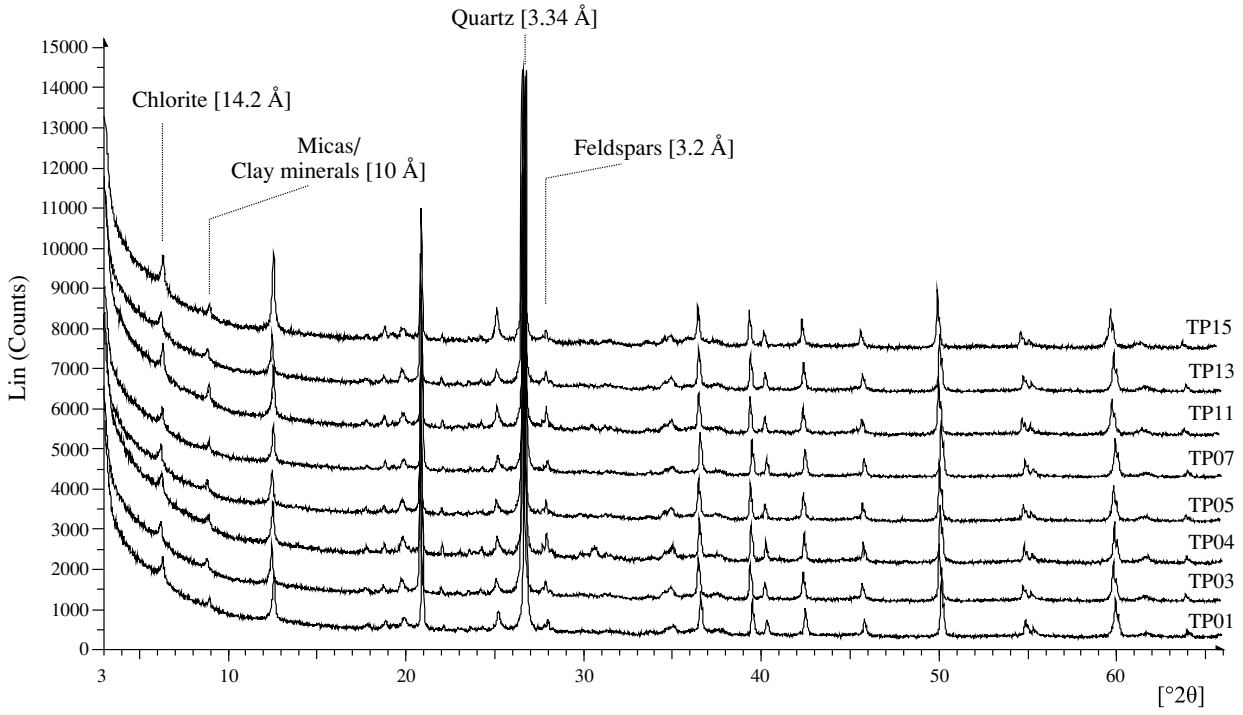

Fig. 5. The XRD patterns of whole-rock shale samples.

for these elements in both F1 and F2.

High field strength elements (HFSE): Y, Zr, Nb, REE, Th, U As for the shales the HFSE have concentrations similar to those of the UCC. The chondrite normalized REE patterns (Fig. 4) have a PAAS-like shape characterized by LREE/HREE fractionation (average $(La/Yb)_{ch} = 9.0 \pm 0.6$) and negative Eu-anomaly (average $Eu/Eu^* = 0.81 \pm 0.10$).

In the Fe- and Mn-rich samples Zr, Nb, Th, U, and LREE are depleted whereas HREE are close to the UCC values. The chondrite normalized REE patterns (Fig. 4) show a limited LREE-HREE fractionation (average $(La/Yb)_{ch} = 3.1 \pm 1.8$) and average negative Eu-anomaly ($Eu/Eu^* = 0.76 \pm 0.10$) similar to that of the shales.

HFSE, with the notably exception of Y and Yb, have high positive weights in the first factor. The linkage between Al_2O_3 and many trace elements does not reflect necessarily a structural control of the clay minerals. HFSE are very dilute in natural waters (e.g., Braun *et al*., 1993) and have, consequently, very low water/rock partition coefficients (Whitfield and Turner, 1979). In shales these elements are generally hosted in accessory phases often observed as inclusions in the mica-like clay minerals (Caggianelli *et al*., 1992; Slack and Stevens, 1994; Mongelli *et al*., 1996). However, Y and Yb have positive weights in the second factor, suggesting the aqueous fraction of these elements should be involved in diagenetic processes and incorporated in secondary phosphate phase.

Transition elements (TE): Sc, V, Cr, Co, Ni, Cu, Zn In the shales, the concentration of the transition metals, including are generally higher than that of the UCC. In the Fe- and Mn-rich samples Sc, V, Cr, Co, and Zn are close to the UCC values whereas Ni and Cu are enriched (Fig. 3b).

V and Cr have strong positive weights in the first factor suggestive of a control by detrital minerals chlorite and micas. For the other TE a lack of significant weights is observed in both factors.

MINERALOGY

The distribution of whole-rock mineralogy along the studied successions is shown in Figs. 5 and 6, and in Table 3.

The whole rock mineralogy of the shales is quite homogeneous (Fig. 5). The XRD whole rock spectrum indicate that these samples are formed by micas/clay minerals, chlorite and quartz prevailing on feldspars.

The Mn-rich samples are generally formed by micas/clay minerals, rhodochrosite, siderite, chlorite and quartz (Fig. 6). The position of the principal peak of rhodochrosite is $31.48°2\theta$, whereas the principal peak of siderite is $32.04°2\theta$. These two phases are clearly recognized on the studied XRD spectrum (Figs. 6 and 7). Siderite is not observed in some Mn-rich-samples (TP14, TP16 and TPCC). The TP02b sample is characterized by

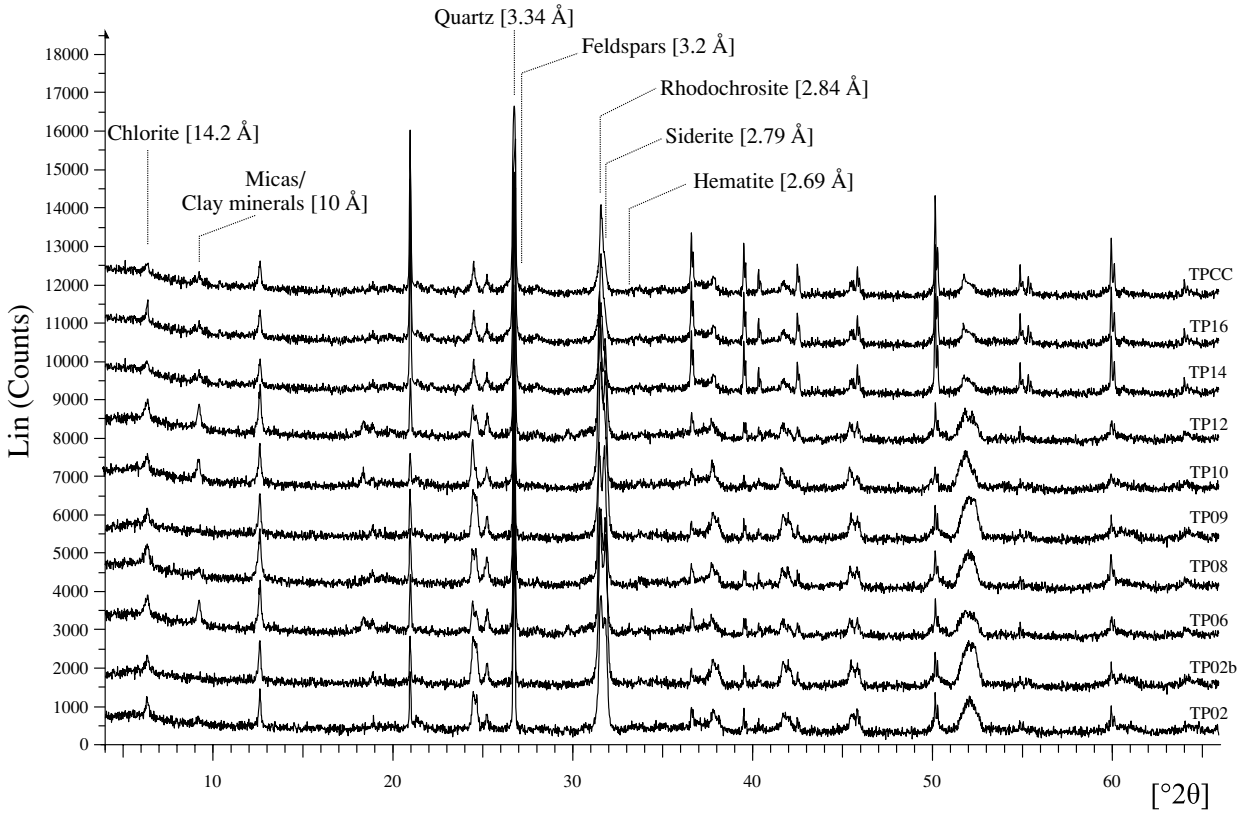

Fig. 6. The XRD patterns of whole-rock Mn-rich samples.

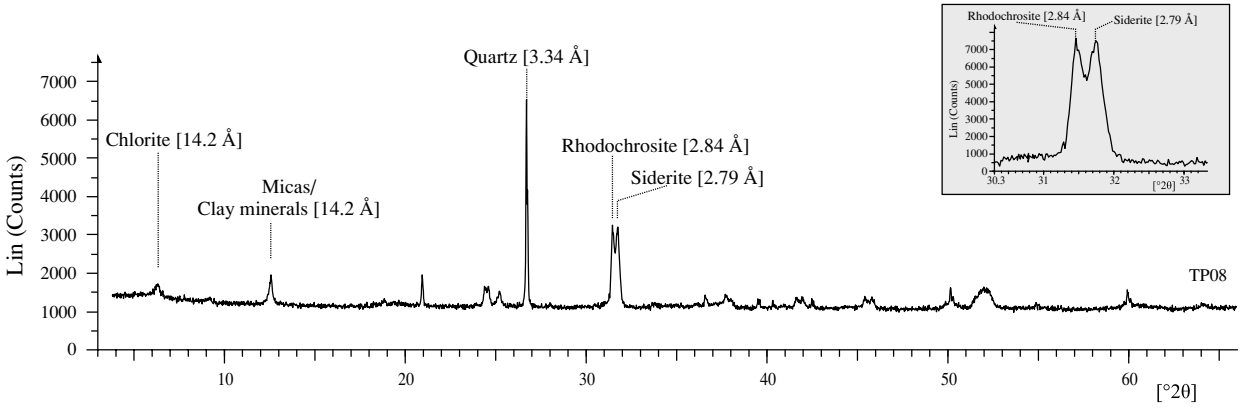

Fig. 7. The XRD patterns of whole-rock TP08 sample, with the very close position of the principal peak of rhodochrosite (31.48°2θ - 2.84 Å) and siderite (32.04°2θ - 2.79 Å).

abundant rhodochrosite and siderite with quartz, chlorite and scarce/negligible amounts of micas/clay minerals. The TP10 sample is enriched in micas/clay minerals and chlorite with abundant rhodochrosite, siderite and quartz (Fig. 6). Low hematite is detected only in the TP06 sample, whereas feldspars in trace are observed only in the TP12 sample (Fig. 6 and Table 3). The TPCC sample and the TP14 sample are very similar with micas/clay minerals and quartz prevailing on rhodochrosite, and traces of chlorite (Fig. 6 and Table 3).

The dominant peak of $FeCO_3$ and $MnCO_3$ are weakly shifted, suggesting Fe partially substituted by Mg, and Mn partially substituted by Ca. These results are comparable with other previous studies on Mn-rich sediments

Table 3. The distribution of whole-rock mineralogy of the studied samples. Samples TP01, TP03, TP04, TP05, TP07, TP11, TP13, TP15 are shales. TP02, TP02b, TP06, TP08, TP09, TP10, TP12, TP14, TP16, TPCC are Mn-rich layers.

Samples	Qtz	Rhod	Sider	Chl	MM/Clay min	Felds	Hem
TP01	+	–	–	+	+	+	–
TP03	+	–	–	+	+	+	–
TP04	+	–	–	+	+	+	–
TP05	+	–	–	+	+	+	–
TP07	+	–	–	+	+	+	–
TP11	+	–	–	+	+	+	–
TP13	+	–	–	+	+	+	–
TP15	+	–	–	+	+	+	–
TP02	+	+	+	+	+	–	–
TP02b	+	+	+	+	+	–	–
TP06	+	+	+	+	+	–	tr
TP08	+	+	+	+	+	–	–
TP09	+	+	+	+	+	–	–
TP10	+	+	+	+	+	–	–
TP12	+	+	+	+	+	tr	–
TP14	+	+	–	tr	+	–	–
TP16	+	+	–	+	+	–	–
TPCC	+	+	–	tr	+	–	–

(e.g., Middelburg *et al*., 1987; Glasby and Schulz, 1999; Haney *et al*., 2006).

Discussion

The behavior of manganese and iron in sedimentary environments is largely controlled by Eh and pH (e.g., Maynard, 2003, and references therein). Eh-pH diagrams suggest that soluble manganese has a larger stability field than soluble iron under moderately reducing conditions. This involves that, below the sediment-water interface, Mn^{2+} is mobilized into the pore water whereas iron is fixed by solid phases. In more reducing marine environments, characterized by low Eh and high sulfur content, iron occurs as sulfide but manganese is still mobile.

Rhodochrosite may form in both anoxic sulfidic and non-sulfidic environments whereas siderite is restricted to anoxic non-sulfidic methanic environments (Berner, 1981). More recently Curtis (1995) suggested that manganese and iron reduction resulting from methanogenesis in the presence of sulphate ions produces rhodochrosite and pyrite, and only in the absence of sulphate ions siderite forms (Carman and Rahm, 1997). Both rhodochrosite and siderite thus occur in rapidly accumulating fine-grained organic-rich sediments, characterized by high alkalinities and high dissolved Mn^{2+} and Fe^{2+}, where CO_2 is produced as a result of oxidation of organic matter (e.g., Schulz *et al*., 1994; Thamdrup *et al*., 1994; Torres *et al*., 1995).

It has to be stressed that most of the Mn–carbonates recognized in marine deposits host considerable amounts

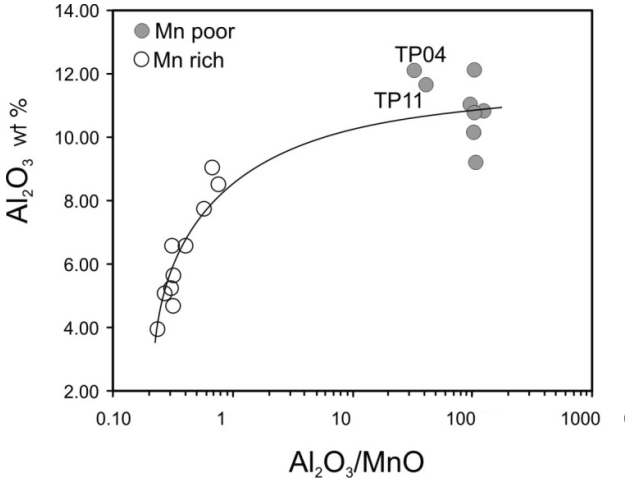

Fig. 8. The Al_2O_3/MnO vs. Al_2O_3 diagram; the carbonate-rich samples fall on the mixing curve having as end members the average shale and the Mn-richest sediment.

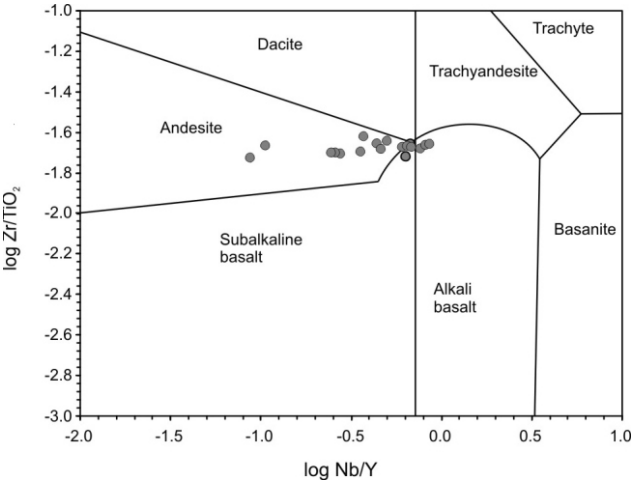

Fig. 9. logZr/TiO_2 vs. logNb/Y diagram; all samples plot on the same trend, which is consistent with everything having the same source.

of calcium (Maynard, 2003). Middelburg *et al*. (1987) suggested that pure $MnCO_3$ cannot form within marine sediments since pore water composition does not lie in a range in which it would be in equilibrium with pure $MnCO_3$. In our case, several observations such as the higher Ca contents in the Mn–Fe rich layers compared to shales, the negative weight of CaO, as MnO in F1, and the lack of calcite, suggest the presence of a mixed Mn–Ca carbonate rather than pure rhodochrosite.

Glasby and Schulz (1999) calculated Eh-pH diagrams for Mn and Fe using element concentrations in bottom seawater and showed that significant differences arise

from standard Eh-pH diagrams, obtained for natural waters at 25°C and 1 bar and assuming an element concentration of 10^{-6} M. They suggested that Ca–rhodochrosite precipitated within the pore waters of reducing sediments since neither rhodochrosite nor siderite can form in equilibrium with bottom seawater. Thus according to Glasby and Schulz (1999) the resulting sediment should be a mixing between the detrital and the authigenic component. Assuming Al_2O_3 as an index for the detrital component, it is clearly envisaged that in the binary Al_2O_3/MnO vs. Al_2O_3 diagram the carbonate-rich samples fall on the mixing curve, between the average shale and the richest MnO sediment (TP10, MnO = 20.53 wt. %; Fig. 8). This supports the idea that carbonate-rich samples formed through precipitation of carbonate minerals in the pore waters of the terrigenous detritus accumulating at the sea bottom as a consequence of diagenetic processes. The source areas of the detrital component of the studied samples have been evaluated by the logZr/TiO_2 vs. logNd/Y diagram (Fig. 9; Floyd and Winchester, 1978). This diagram shows that all samples plot on the same trend, indicating the same source material. This also supports a subduction-zone setting, perhaps a retro-arc foreland, as an appropriate tectonic setting for the source area (Floyd and Winchester, 1978; Winchester and Floyd, 1977).

Unaltered marine carbonates are expected to preserve the chemical characteristics of ambient seawater, such as the REE distribution (e.g., Tanaka and Kawabe, 2006). Carbonate-rich samples normalized to fine-grained siliciclastis sediments, have typical HREE enrichment, negative Ce-anomaly, and lower total REE (e.g., McLennan, 1989 and references therein). Normalizing the carbonate-rich samples to the average composition of the interbedded free-carbonate shale, we observe HREE enrichments ($(La/Yb)_{shale}$ ranges from 0.17 to 0.86), lower total REE contents, and the lack of negative Ce-anomaly (1.06 to 1.35). It is well known that cerium in seawater shows a negative anomaly due to the Ce^{3+} oxidation to Ce^{4+} under the oceanic oxidizing conditions (e.g., Maynard, 2003). In anoxic waters trivalent cerium is stable (Wignall, 1994) and in alkaline to very alkaline conditions $CeCO_3^+$, $Ce(CO_3)_2^-$ and $Ce(OH)_2^+$ are the dominant species (de Baar *et al*., 1988) similarly to that observed in seawater for the other trivalent REE where dominant species are $LnCO_3^+$ and $Ln(CO_3)_2^-$ (Byrne and Sholkovitz, 1996; Ohta and Kawabe, 2000). The lack of negative Ce-anomaly relative to the shales, indicates that Mn- and Fe-carbonate most likely formed under anoxic conditions.

As previously stated, the occurrence of both rhodocrosite and siderite is restricted to fine-grained, rapidly accumulating sediments where CO_2 derives from oxidation of organic matter. Such sediments have to be characterized by high alkalinities and high dissolved Mn^{2+} and Fe^{2+}. Anoxic pore waters can have alkalinities nearly two orders of magnitude higher than in the overlying seawater (Schulz *et al*., 1994). Further, Calvert and Pedersen (1996) assumed that carbonates precipitated in anoxic conditions, in subsurface sediments only when bottom seawater is oxic enough to cause the accumulation of Mn– and Fe–oxyhydroxides in surface sediments. Thus it is suggested that the occurrence of Ca–rhodochrosite is a reliable index of sedimentation under oxygenated bottom water conditions.

The mineralization is enhanced if the site of accumulation is protected from dilution by clastic sediment input (Robb, 2004). The alternation between Mn– and Fe–carbonate silts and carbonate-free shales along the studied sedimentary succession, may be controlled by various geological parameters, such as the cyclic deposition of carbonate sediments controlled by eustatic sea-level oscillations (e.g., Osleger and Read, 1991), as observed in the western Tethys during middle and late Triassic (Goldhammer *et al*., 1990). Under these conditions sudden, vertical lithology changes as well as the occurrence of centimetric-scaled iron and manganese concentrations may occur (Varol and Tunay, 1996). Thus Triassic eustatic sea-level fluctuations likely controlled the alternation of Mn– and Fe–carbonate silts and carbonate-free shales in our succession.

SUMMARY

1. Alternation of Mn-rich layers, formed by micas/clay minerals, mixed Mn–Ca carbonate, siderite, chlorite and quartz, and shales has been recognized in a natural section of the Northern-Calabrian Units in southern Italy.
2. The carbonate-rich samples formed through precipitation of carbonate minerals in the pore waters of the terrigenous detritus accumulating at the sea bottom.
3. Normalizing the carbonate-rich samples to the average composition of the interbedded free-carbonate shale, we observe HREE enrichment, lower total REE contents, and the lack of negative Ce-anomaly supporting the idea of an anoxic environment of formation.
4. The alternation between Mn– and Fe–carbonate silts and carbonate-free shales along the studied sedimentary succession was likely controlled by eustatic sea-level oscillations that in middle and late Triassic in the western Tethys are well documented.

Acknowledgments—This work was founded by the MIUR-PRIN 2001–2003 Project (Age and sedimentary characters of the Mesozoic continental redbeds (Verrucano) from Northern Apennines to the Betic Cordillera: implications for paleogeographic and tectonic evolution of the central-western Mediterranean Alpine Belts; Resp. S. Critelli, G. Mongelli, V. Perrone), MIUR-ex60% Projects (Paleogeographic and Paleotectonic Evolution of the Circum-Mediterranean Orogenic

Belts, 2001–2005; and Relationships between Tectonic Accretion, Volcanism and Clastic Sedimentation within the Circum-Mediterranean Orogenic Belts, 2006; Resp. S. Critelli), and the 2006–2008 MIUR-PRIN Project 2006.04.8397 "The Cenozoic clastic sedimentation within the circum-Mediterranean orogenic belts: implications for paleogeographic and paleotectonic evolution" (Resp. S. Critelli, G. Mongelli, V. Perrone). H. Öztürk, J. B. Maynard and B. Orberger reviewed the manuscript and provided many helpful comments.

REFERENCES

Amirbahman, A., Schoenberger, R., Johnson, C. and Sigg, L. (1998) Aqueous- and solid-phase biogeochemistry of a calcareous aquifer system downgradient from a municipal solid waste landfill (Winterthur, Switzerland). *Environ. Sci. Technol.* **32**, 1933–1940.

Assorgia, A., Barca, S., Casula, G. and Spano, C. (1988) Le successioni sedimentarie e vulcaniche del Miocene nei dintorni di Giave e Cossoine (Logudoro, Sardegna NW). *Boll. Soc. Sarda Sc. Nat.* **26**, 75–107.

Beccaluva, L., Gabbianelli, G., Lucchini, F., Rossi, P. L. and Savelli, C. (1985) Petrology and K/Ar age of volcanics dredged from the Aeolian seamounts: implications for geodynamics evolution of the southern Tyrrhenian basin. *Earth Planet. Sci. Lett.* **74**, 187–208.

Berner, R. A. (1981) A new geochemical classification of sedimentary environments. *J. Sed. Petrol.* **51**, 359–365.

Bolton, B. R. and Frakes, L. A. (1985) Geology and genesis of manganese oolite, Chiatura, Georgia, USSR. *Geol. Soc. Am. Bull.* **96**, 1398–1406.

Bonatti, E., Zerbi, M., Kay, R. and Rydell, H. (1976) Metalliferous deposits from the Apennine ophiolites: Mesozoic equivalents of modern deposits from oceanic spreading centers. *Geol. Soc. Am. Bull.* **87**, 83–94.

Boni, M. and di Nocera, S. (1977) The geological significance of the manganese-ore mineral facies in the Miocene of the Matese Mountains (Central-Southern Apennines, Italy). *Min. Dep.* **12**, 281–292.

Braun, J. J., Pagel, M., Herbillon, A. and Rosin, C. (1993) Mobilization and redistribution of REEs and thorium in a syenitic lateritic profile: A mass balance study. *Geochim. Cosmochim. Acta* **57**, 4419–4434.

Byrne, R. H. and Sholkovitz, E. R. (1996) Marine chemistry and geochemistry of the lanthanides. *Handbook on the Physics and Chemistry of Rare Earths*, Vol. 23 (Gschneidner, K. A., Jr. and Eyring, L. R., eds.), 497–593, Elsevier Sciences B.V.

Caggianelli, A., Fiore, S., Mongelli, G. and Salvemini, A. (1992) REE distribution in the clay fraction of pelites from the southern Apennines, Italy. *Chem. Geol.* **99**, 253–263.

Calvert, S. E. and Pedersen, T. F. (1996) Sedimentary geochemistry of manganese: implications for the environments of formation of manganiferous black shales. *Econ. Geol.* **91**, 36–46.

Carman, R. and Rahm, L. (1997) Early diagenesis and chemical characteristics of interstitial water and sediments in the deep deposition bottoms of the Baltic proper. *J. Sea Res.* **37**, 25–47.

Cello, G., Invernizzi, C. and Mazzoli, S. (1996) Structural segnature of tectonic processes in the calabrian Arc, southern Italy: evidence from the oceanic-derived Diamanteterranova unit. *Tectonics* **15**, 187–200.

Critelli, S. (1993) Sandstone detrital modes in the Paleogene Liguride Complex, accretionary wedge of the southern Apennines (Italy). *J. Sed. Petrol.* **63**, 464–476.

Critelli, S. (1999) The interplay of lithospheric flexure and thrust accomodation in forming stratigraphic sequences in the Southern Apennines foreland basin system, Italy. *Accad. Naz. Lin., Rend. Lin. Sci. Fis. Nat.* **IX**(10), 257–326.

Critelli, S. and Le Pera, E. (1998) Post-Oligocene sediment-dispersal systems and unroofing history of the Calabrian microplate, Italy. *Intern. Geol. Rev.* **40**, 609–637.

Curtis, C. D. (1995) Post-depositional evolution of mudstones 1: early days and parental influences. *J. Geol. Soc. Lond.* **152**, 577–586.

Dasgupta, S., Roy, S. and Fukuoka, M. (1992) Depositional models for manganese oxide and carbonate deposits of the Precambrian Sausar Group, India. *Econ. Geol.* **87**, 1412–1418.

Davis, J. C. (1986) *Statistics and Data Analysis in Geology*. Wiley & Sons, New York.

de Baar, H. J. W., German, C. R., Elderfield, H. and Van Gaans, P. (1988) Rare earth element distribution in anoxic waters of the Cariaco Trench. *Geochim. Cosmochim. Acta* **52**, 1203–1219.

Doglioni, C., Harabaglia, P., Martinelli, G., Mongelli, F. and Zito, G. (1996) A geodynamic model of the Southern Apennines. *Terra Nova* **8**, 540–547.

Dresel, P. E. (1989) The dissolution kinetics of siderite and its effect on acid mine drainage. Ph.D. thesis. Pennsylvania State University.

Duff, M. L., Coughlin, J. J. and Hunter, D. B. (2002) Uranium coprecipitation with iron oxide minerals. *Geochim. Cosmochim. Acta* **66**, 3533–3549.

Fan, D., Yang, P. and Wang, R. (1999) Characteristics and origin of the Middle Proterozoic Dongshuichang chambersite deposit, Jixian, Tianjiin, China. *Ore Geol. Rev.* **15**, 135–151.

Floyd, P. A. and Winchester, J. A. (1978) Identification and discrimination of altered and metamorphosed volcanic rocks using immobile elements. *Chem. Geol.* **21**, 291–306.

Föllmi, K. B. (1996) The phosphorus cicle, phosphogenesis and marine phosphate-rich deposits. *Earth-Sci. Rev.* **40**, 55–124.

Force, E. R. and Cannon, W. F. (1988) Depositional model for shallow marine manganese deposits around black shale basins. *Econ. Geol.* **83**, 93–117.

Franzini, M., Leoni, L. and Saitta, M. (1972) A simple method to evaluate the matrix effects in X-ray fluorescence analysis. *X-ray spectrometry* **1**, 151–154.

Franzini, M., Leoni, L. and Saitta, M. (1975) Revisione di una metodologia analitica per fluorescenza X basata sulla correzione degli effetti di matrice. *Rend. Soc. It. Min. Petr.* **31**, 365–378.

Glasby, G. P. and Schulz, H. D. (1999) Eh, pH diagrams for Mn, Fe, Co, Ni, Cu and As under seawater conditions: Application of two new types of Eh, pH diagrams to the study of specific problems in marine geochemistry. *Aquatic*

Geochem. **5**, 227–248.

Goldhammer, R. K., Dunn, P. A. and Hardie, L. A. (1990) Depositional cycles, composite sea-level changes, cycle stacking patterns, and the hierarchy of stratigraphic forcing: examples from Alpine Triassic platform carbonates. *Geol. Soc. Am. Bull.* **102**, 535–562.

Haney, E. B., Haney, R. L., Hossner, L. R. and White, G. N. (2006) Neutralization potential determination of siderite ($FeCO_3$) using selected oxidants. *J. Environ. Qual.* **35**, 871–879.

Hem, J. D. (1978) Redox processes at surfaces of manganese oxide and their effects on aqueous metal ions. *Chem. Geol.* **21**, 199–218.

Hem, J. D., Lind, C. J. and Roberson, C. E. (1989) Coprecipitation and redox reactions of manganese oxides with copper and nickel. *Geochim. Cosmochim. Acta* **53**, 2811–2822.

Jenkyns, H. C. (1988) The early Toarcian (Jurassic) anoxic event: stratigraphic, sedimentary and geochemical evidence. *Am. J. Sci.* **288**, 101–151.

Jensen, D. L., Boddum, J. V., Tjell, J. L. and Christensen, T. H. (2002) The solubility of rhodochrosite ($MnCO_3$) and siderite ($FeCO_3$) in anaerobic aquatic environments. *Appl. Geochem.* **17**, 503–511.

Kelts, K. (1998) Environments of deposition of lacustrine petroleum source rocks: An introduction. *Lacustrine Petroleum Source Rocks* (Fleet, A., Kelts, K. and Talbot, M., eds.), 3–26, Geological Society of America.

La Force, M., Hansel, C. and Ferdoff, S. (2002) Seasonal transformations of manganese in a palustrine emergent wetland. *Soil Sci. Am. J.* **66**, 1377–1389.

Leoni, L. and Saitta, M. (1976) X-ray fluorescence analysis of 29 trace elements in rock and mineral standards. *Rend. Soc. It. Min. Petr.* **32**, 497–510.

Marchesini, M. and Pagano, R. (2001) The Val Graveglia manganese district, Liguria, Italy. *Mineral. Rec.* **32**, 349–379.

Maynard, J. B. (2003) Manganiferous sediments, rocks, and ores. *Treatise on Geochemistry*, Vol. 7 (Holland, H. D. and Turekian, K. K., eds.), 289–308, Elsevier.

McLennan, S. M. (1989) Rare earth elements in sedimentary rocks: influence of provenance and sedimentary processes. *Geochemistry and Mineralogy of Rare Earth Elements* (Lipin, B. R. and McKay, G. A., eds.), *Min. Soc. Am. Rev. Mineral.* **21**, 169–200.

McMillan, S. and Schwertmann, U. (1998) Morphological and genetic relations between siderite, calcite, and goethite in a low moor peat from southern Germany. *Eur. J. Soil Sci.* **49**, 283–293.

Middelburg, J., De Lange, G. and Van Der Weijden, C. (1987) Manganese solubility control in marine porewaters. *Geochim. Cosmochim. Acta* **51**, 759–763.

Monaco, C., Tortorici, L., Morten, L., Critelli, S. and Tansi, C. (1995) Geologia del versante nord-orientale del Massiccio del Pollino (confine Calabro-Lucano): nota illustrativa sintetica della carta geologica alla scala 1:50.000. *Boll. Soc. Geol. It.* **114**, 277–291.

Mongelli, G. and Dinelli, E. (2001) The geochemistry of shales from the "Frido Unit", Liguride Complex, Lucanian Apennines, Italy: implications for provenance and tectonic setting. *Ofioliti* **26**, 457–466.

Mongelli, G., Cullers, R. and Muelheisen, S. (1996) Geochemistry of Cenozoic shales from the Varicolori Formation, Southern Apennines, Italy: implications for mineralogical, grain size control and provenance. *Eur. J. Mineral.* **8**, 733–754.

Morgan, J. (1967) Chemical equilibria and kinetic properties of manganese in natural water. *Principles and Applications of Water Chemistry* (Faust, S. and Hunter J., eds.), 561–623, Wiley.

Ogniben, L. (1969) Schema introduttivo alla geologia del confine calabro-lucano. *Mem. Soc. Geol. It.* **8**, 453–763.

Ohta, A. and Kawabe, I. (2000) Theoretical study of tetrad effects observed in REE distribution coefficients between marine Fe–Mn deposit and deep seawater, and in REE(III)-carbonate complexation constants. *Geochem. J.* **34**, 455–473.

Osleger, D. and Read, J. F. (1991) Relation of eustasy to stacking patterns of meter-scale carbonate cycles, Late Cambrian, USA. *J. Sed. Petrol.* **61**, 1225–1252.

Öztürk, H. and Hein, J. R. (1997) Mineralogy and stable isotopes of black shale-hosted manganese ores, southwestern Taurides. Turkey. *Econ. Geol.* **92**, 733–744.

Patacca, E. and Scandone, P. (2007) Geology of the Southern Apennines. *Results of the CROP Project, Sub-project CROP-04 So* (Mazzotti, A., Patacca, E. and Scandone, P., eds.), Spec. Issue **7**, 75–119.

Pedersen, T. F. and Calvert, S. E. (1990) Anoxia vs. productivity: what controls the formation of organic-carbon-rich sediments and sedimentary rocks? *Am. Ass. Petrol. Geol. Bull.* **74**, 454–466.

Pescatore, T., Renda, P., Schiattarella, M. and Tramutoli, M. (1999) Stratigraphic and structural relationship between Meso–Cenozoic Lagonegro basin and coeval carbonate plataforms in Southern Apennines, Italy. *Tectonophysics* **315**, 269–286.

Robb, L. (2004) *Introduction to Ore-Forming Processes*. Wiley-Blackwell, Oxford.

Rudnick, R. L. and Fountain, D. M. (1995) Nature and composition of the continental crust: a lower crustal perspective. *Rev. Geophys.* **33**, 267–309.

Scandone, P. (1972) Studi di geologia lucana: Carta dei terreni della serie calcareo-silicomarnosa e note illustrative. *Boll. Soc. Natur. In Napoli* **81**, 225–300.

Schulz, H. D., Dahmke, A., Schinzel, U., Wallmann, K. and Zabel, M. (1994) Early diagenetic processes, fluxes, and reaction rates in sediments of the South Atlantic. *Geochim. Cosmochim. Acta* **58**, 2041–2060.

Sgrosso, I. (1986) Criteri ed elementi per una ricostruzione paleogeografica delle zone esterne dell'Appennino centromeridionale. *Mem. Soc. Geol. It.* **35**, 203–219.

Slack, J. F. and Stevens, B. P. J. (1994) Clastic metasediments of the Early Proterozoic Broken Hill Group, New South Wales, Australia: Geochemistry, provenance, and metallogenic significance. *Geochim. Cosmochim. Acta* **58**, 3633–3652.

Tanaka, K. and Kawabe, I. (2006) REE abundances in ancient seawater inferred from marine limestone and experimental REE partition coefficients between calcite and aqueous so-

lution. *Geochem. J.* **40**, 425–435.
Taylor, S. R. and McLennan, S. M. (1985) *The Continental Crust; Its Composition and Evolution*. Blackwell, Oxford.
Thamdrup, B., Fossing, H. and Jorgensen, B. B. (1994) Manganese, iron and sulfur cycling in a coastal marine sediment, Aarhus Bay, Denmark. *Geochim. Cosmochim. Acta* **58**, 5115–5129.
Torres, M. E., Marsaglia, K. M., Martin, J. B. and Murray, R. W. (1995) Sediment diagenesis in western Pacific Basins. *Active Marginal Basins of the Western Pacific* (Taylor, B. and Natland, J., eds.), *Am. Geophys. Un. Geophys. Monogr.* **88**, 241–258.
Varol, B. and Tunay, G. (1996) Description and internal structure of the condensate series: an example from the Beysehir-Hoyran Nappe. *Mineral Res. Expl. Bull.* **118**, 15–24.
Whitfield, M. and Turner, D. R. (1979) Water-rock partition coefficients and the composition of seawater and river water. *Nature* **278**, 132–137.
Wignall, P. B. (1994) *Black Shales*. Oxford monographs on geology and geophysics, Oxford Science Publications.
Winchester, J. A. and Floyd, P. A. (1977) Geochemical discrimination of different magma series and their differentiation products using immobile elements. *Chem. Geol.* **20**, 325–343.
Yeh, H. W., Hein, J. R., Ye, J. and Fan, D. (1999) Stable isotope, chemical, and mineral compositions of the Middle Proterozoic Lijiaying Mn deposit, Shaanxi Province, China. *Ore Geol. Rev.* **15**, 55–69.
Zeng, Y. and Liu, T. (1999) Characteristics of the Devonian Xialei manganese deposit, Guangxi Zhuang Autonomous Region, China. *Ore Geol. Rev.* **15**, 153–163.